

This is a repository copy of *Search for the η mesic ^3He in the $d p \rightarrow d p \pi^0$ reaction with the WASA-at-COSY facility.*

White Rose Research Online URL for this paper:

<https://eprints.whiterose.ac.uk/183247/>

Article:

(2020) Search for the η mesic ^3He in the $d p \rightarrow d p \pi^0$ reaction with the WASA-at-COSY facility. Phys. Rev. C. ISSN 2469-9993

<https://doi.org/10.1103/PhysRevC.102.044322>

Reuse

Items deposited in White Rose Research Online are protected by copyright, with all rights reserved unless indicated otherwise. They may be downloaded and/or printed for private study, or other acts as permitted by national copyright laws. The publisher or other rights holders may allow further reproduction and re-use of the full text version. This is indicated by the licence information on the White Rose Research Online record for the item.

Takedown

If you consider content in White Rose Research Online to be in breach of UK law, please notify us by emailing eprints@whiterose.ac.uk including the URL of the record and the reason for the withdrawal request.

Search for the η mesic ^3He in the $pd \rightarrow dp\pi^0$ reaction with the WASA-at-COSY facility

P. Adlarson,¹ W. Augustyniak,² M. Bashkanov,³ S. D. Bass,^{4,5} F.S. Bergmann,⁶ M. Berłowski,⁷ A. Bondar,^{8,9}
M. Büscher,^{10,11} H. Calén,¹ I. Ciepał,¹² H. Clement,^{13,14} E. Czerwiński,⁴ K. Demmich,⁶ R. Engels,¹⁵
A. Erven,¹⁶ W. Erven,¹⁶ W. Eyrych,¹⁷ P. Fedorets,^{15,18} K. Föhl,¹⁹ K. Fransson,¹ F. Goldenbaum,¹⁵
A. Goswami,^{20,15} K. Grigoryev,^{15,21} L. Heijmanskjöld,^{1,*} V. Hejny,¹⁵ N. Hüskens,⁶ S. Hirenzaki,²² T. Johansson,¹
B. Kamys,⁴ N. G. Kelkar,²³ G. Kemmerling,^{16,†} A. Khokkaz,⁶ A. Khreptak,⁴ D. A. Kirillov,²⁴ S. Kistryn,⁴
H. Kleines,^{16,†} B. Kłos,²⁵ W. Krzemień,²⁶ P. Kulessa,¹² A. Kupś,^{1,7} K. Lalwani,²⁷ D. Lersch,^{15,‡}
B. Lorentz,¹⁵ A. Magiera,⁴ R. Maier,^{15,28} P. Marciniowski,¹ B. Mariański,² H.-P. Morsch,² P. Moskal,⁴
H. Ohm,¹⁵ W. Parol,⁴ E. Perez del Rio,^{13,14} N. M. Piskunov,²⁴ D. Prasuhn,¹⁵ D. Pszczel,^{1,7} K. Pysz,¹²
J. Ritman,^{15,28,29} A. Roy,²⁰ O. Rundel,⁴ S. Sawant,³⁰ S. Schadmand,¹⁵ T. Sefzick,¹⁵ V. Serdyuk,¹⁵
B. Schwartz,^{8,9} T. Skorodko,^{13,14,31} M. Skurzok,^{4,§} J. Smyrski,⁴ V. Sopov,¹⁸ R. Stassen,¹⁵ J. Stepaniak,⁷
E. Stephan,²⁵ G. Sterzenbach,¹⁵ H. Stockhorst,¹⁵ H. Ströher,^{15,28} A. Szczurek,¹² M. Wolke,¹ A. Wrońska,⁴
P. Wüstner,¹⁶ A. Yamamoto,³² J. Zabierowski,³³ M.J. Zieliński,⁴ J. Złomańczuk,¹ and M. Żurek^{15,¶}

(WASA-at-COSY Collaboration)

- ¹Division of Nuclear Physics, Department of Physics and Astronomy, Uppsala University, Box 516, 75120 Uppsala, Sweden
²Department of Nuclear Physics, National Centre for Nuclear Research, Ludwika Pasteura 7, 02-093, Warsaw, Poland
³School of Physics and Astronomy, University of Edinburgh, James Clerk
Maxwell Building, Peter Guthrie Tait Road, Edinburgh EH9 3FD, Great Britain
⁴Institute of Physics, Jagiellonian University, prof. Stanisława Łojasiewicza 11, 30-348 Kraków, Poland
⁵Kitzbühel Centre for Physics, Kitzbühel, Austria
⁶Institut für Kernphysik, Westfälische Wilhelms-Universität Münster, Wilhelm-Klemm-Str. 9, 48149 Münster, Germany
⁷High Energy Physics Department, National Centre for Nuclear Research, Ludwika Pasteura 7, 02-093, Warsaw, Poland
⁸Budker Institute of Nuclear Physics of SB RAS, 11 akademika Lavrentieva prospect, Novosibirsk, 630090, Russia
⁹Novosibirsk State University, 2 Pirogova Str., Novosibirsk, 630090, Russia
¹⁰Peter Grünberg Institut, PGI-6 Elektronische Eigenschaften, Forschungszentrum Jülich, 52425 Jülich, Germany
¹¹Institut für Laser- und Plasmaphysik, Heinrich-Heine Universität Düsseldorf, Universitätsstr. 1, 40225 Düsseldorf, Germany
¹²The Henryk Niewodniczański Institute of Nuclear Physics, Polish
Academy of Sciences, 152 Radzikowskiego St, 31-342 Kraków, Poland
¹³Physikalisches Institut, Eberhard-Karls-Universität Tübingen, Auf der Morgenstelle 14, 72076 Tübingen, Germany
¹⁴Kepler Center für Astro- und Teilchenphysik, Physikalisches Institut der
Universität Tübingen, Auf der Morgenstelle 14, 72076 Tübingen, Germany
¹⁵Institut für Kernphysik, Forschungszentrum Jülich, 52425 Jülich, Germany
¹⁶Zentralinstitut für Elektronik, Forschungszentrum Jülich, 52425 Jülich, Germany
¹⁷Physikalisches Institut, Friedrich-Alexander-Universität
Erlangen-Nürnberg, Erwin-Rommel-Str. 1, 91058 Erlangen, Germany
¹⁸Institute for Theoretical and Experimental Physics named by A.I. Alikhanov of National
Research Centre “Kurchatov Institute”, 25 Bolshaya Cheremushkinskaya, Moscow, 117218, Russia
¹⁹II. Physikalisches Institut, Justus-Liebig-Universität Gießen, Heinrich-Buff-Ring 16, 35392 Giessen, Germany
²⁰Department of Physics, Indian Institute of Technology Indore, Khandwa Road, Indore-452017, Madhya Pradesh, India
²¹High Energy Physics Division, Petersburg Nuclear Physics Institute named by B.P. Konstantinov of National
Research Centre “Kurchatov Institute”, 1 mkr. Orlova roshcha, Leningradskaya Oblast, Gatchina, 188300, Russia
²²Department of Physics, Nara Women’s University, Nara 630-8506, Japan
²³Departamento de Física, Universidad de los Andes, Cra. 1E, 18A-10, Bogotá, Colombia
²⁴Veksler and Baldin Laboratory of High Energy Physics, Joint
Institute for Nuclear Physics, 6 Joliot-Curie, Dubna, 141980, Russia
²⁵August Chelkowski Institute of Physics, University of Silesia, Uniwersytecka 4, 40-007, Katowice, Poland
²⁶High Energy Physics Division, National Centre for Nuclear Research, 05-400 Otwock-Āźwierk, Poland
²⁷Department of Physics, Malaviya National Institute of Technology Jaipur, JLN Marg Jaipur - 302017, Rajasthan, India
²⁸JARA-FAME, Jülich Aachen Research Alliance, Forschungszentrum
Jülich, 52425 Jülich, and RWTH Aachen, 52056 Aachen, Germany
²⁹Institut für Experimentalphysik I, Ruhr-Universität Bochum, Universitätsstr. 150, 44780 Bochum, Germany
³⁰Department of Physics, Indian Institute of Technology Bombay, Powai, Mumbai-400076, Maharashtra, India
³¹Department of Physics, Tomsk State University, 36 Lenina Avenue, Tomsk, 634050, Russia
³²High Energy Accelerator Research Organisation KEK, Tsukuba, Ibaraki 305-0801, Japan
³³Department of Cosmic Ray Physics, National Centre for Nuclear Research, ul. Uniwersytecka 5, 90-950 Łódź, Poland

(Dated: September 29, 2020)

The excitation function for the $pd \rightarrow dp\pi^0$ reaction has been measured by WASA-at-COSY experiment with the aim of searching for ${}^3\text{He}\text{-}\eta$ mesic nuclei. The measurement in the vicinity of η meson production was performed using a ramped proton beam. The data analysis and interpretation was carried out with the assumption that the η -mesic Helium decays via the formation of an intermediate $N^*(1535)$ resonance. No direct signal of the η -mesic nucleus is observed in the excitation function. We determine a new improved upper limit for the total cross section for the bound state production and decay in the $pd \rightarrow ({}^3\text{He}\text{-}\eta)_{\text{bound}} \rightarrow dp\pi^0$ process. It varies between 13 nb to 24 nb for the bound state with width in the range $\Gamma \in (5, 50)$ MeV.

PACS numbers: 21.85.+d, 21.65.Jk, 25.80.-e, 13.75.-n

Keywords: mesic nuclei, η -mesic nucleus, η meson

I. INTRODUCTION

In this paper we present a new high statistics search for ${}^3\text{He}\text{-}\eta$ bound states with focus on the $pd \rightarrow dp\pi^0$ reaction. The measurement was performed using data from the WASA-at-COSY experiment at Forschungszentrum Jülich. Strong attractive interactions between the η meson and nucleons mean that there is a chance to form η meson bound states in nuclei [1]. If discovered in experiments, these mesic nuclei would be a new state of matter bound just by the strong interaction without electromagnetic Coulomb effects playing a role because of the zero electric charge of the η meson. Early experiments with low statistics using photon [2, 3], pion [4], proton [5] or deuteron [6–8] beams gave hints for possible η mesic bound states but no clear signal [9, 10]. The new results reported here are complementary to the recent ${}^3\text{He}\text{-}\eta$ bound state search using the $pd \rightarrow {}^3\text{He}2\gamma$ and $pd \rightarrow {}^3\text{He}6\gamma$ reactions and performed with the same experiment.

The key physical process involves a virtual η meson produced in the pd collision forming a bound state with the ${}^3\text{He}$ nucleus in which it is produced. The bound states might form by the attractive interaction, with finite width corresponding to the finite lifetime of the state due to the absorptive interaction with the nucleus. η meson interactions with nucleons and nuclei are a topic of much experimental and theoretical interest. For recent reviews see [9–14].

Hints for possible η helium bound states are inferred from the observation of strong interaction in the η helium system. One finds a sharp rise in the cross section at threshold for η production in photoproduction from ${}^3\text{He}$ [2, 15] and in the proton-deuteron reaction

$dp \rightarrow {}^3\text{He}\eta$ [16]. These observations may hint at a reduced η effective mass in the nuclear medium, see e.g. [11].

Possible η -nucleus binding energies are related to the η -nucleus optical potential and to the value of η -nucleon scattering length $a_{\eta N}$ [17]. Phenomenological estimates for the real part of $a_{\eta N}$ are typically between 0.2 and 1 fm. η bound states in helium require a large η -nucleon scattering length with real part greater than about 0.7–1.1 fm [18–20]. Recent calculations in the framework of optical potential [21], multi-body calculations [19], and pionless effective field theory [18] suggest a possible ${}^3\text{He}\text{-}\eta$ bound state.

The related system of η' -nucleus interactions is also a strong candidate for a meson-nucleus bound state. Recent measurements by the CBELSA/TAPS collaboration in Bonn using photoproduction of η' mesons from a carbon target determined the η' -nucleus optical potential $V_{\text{opt}} = V + iW$ with the strength of the real part at nuclear matter density ρ_0 related to the meson's effective mass shift $V = m^* - m = -37 \pm 10 \pm 10$ MeV and imaginary part $W = -10 \pm 2.5$ MeV at ρ_0 [22]. With the attractive real part of the potential greater than the imaginary part, this result has inspired a program of bound state searches with first results (ruling out much larger potential depths) reported in Ref. [23] and future more accurate measurements in planning. The η' mass shift suggested by CBELSA/TAPS is very close to the prediction of the Quark Meson Coupling model, QMC, with mixing angle -20 degrees [24, 25] and consistent with η' -nucleon scattering length determinations from Bonn [26] and COSY-11 [27]. The QMC model predicts an η nucleus potential depth about -100 MeV at ρ_0 .

In May 2014 the experimental search for η mesic ${}^3\text{He}$ nuclei was carried out using the WASA-at-COSY detection system [28–33] at Forschungszentrum Jülich in Germany colliding the COSY proton beam with a deuteron pellet target. The search for η -mesic bound states was performed considering two main predicted mechanisms for the η -mesic bound state decay, via the formation of an intermediate $N^*(1535)$ resonance and its decay into a nucleon pion pair (used in previous experimental studies) and via decay of η -meson still “orbiting” around the nucleus [34]. The bound state, if it exists, would be manifest as a resonance structure in the excitation function for the studied processes below the $pd \rightarrow {}^3\text{He}\eta$ reaction

*Current address: Institut für Kernphysik, Johannes Gutenberg-Universität Mainz, Johann-Joachim-Becher Weg 45, 55128 Mainz, Germany

†Current address: Jülich Centre for Neutron Science JCNS, Forschungszentrum Jülich, 52425 Jülich, Germany

‡Current address: Department of Physics, Florida State University, 77 Chieftan Way, Tallahassee, FL 32306-4350, USA

§Current address: INFN, Laboratori Nazionali di Frascati, Via E. Fermi, 40, 00044 Frascati (Roma), Italy

¶Current address: Lawrence Berkeley National Laboratory, Berkeley, California 94720

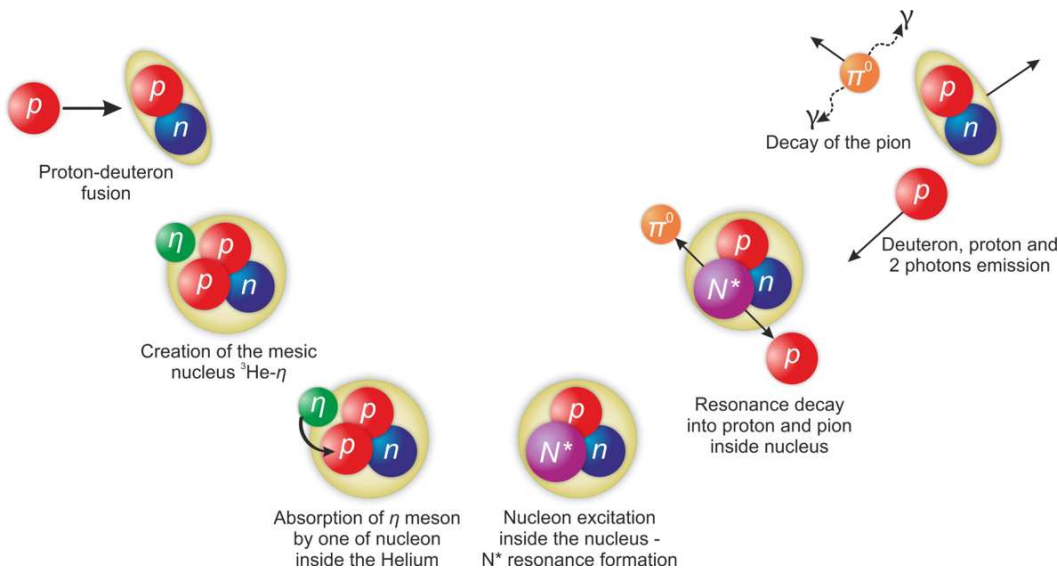


FIG. 1: (Color online) Model of the ${}^3\text{He}\text{-}\eta$ bound state production and decay in the $pd \rightarrow dp\pi^0$ reaction.

threshold.

The mechanism of η -mesic ${}^3\text{He}$ decay has been investigated recently for the first time by analysing the $pd \rightarrow {}^3\text{He}2\gamma$ and $pd \rightarrow {}^3\text{He}6\gamma$ reactions [35] assuming the theoretical model recently developed in [34]. The final excitation functions for both channels showed a slight indication of the signal from a possible bound state for $\Gamma > 20$ MeV and binding energies in the range from 0 to 15 MeV which is, however, covered by the systematic error. Therefore, drawing conclusions for the bound state existence in the considered mechanism was not possible. The upper limit at the CL=90% obtained by fitting simultaneously excitation functions for both processes varied between 2 nb to 15 nb depending on the bound state parameters [35].

In this paper we present results of the search for η -mesic ${}^3\text{He}$ in the $pd \rightarrow dp\pi^0$ reaction corresponding to the mechanism $pd \rightarrow ({}^3\text{He}\text{-}\eta)_{\text{bound}} \rightarrow N^*d \rightarrow dp\pi^0$ via excitation of the $N^*(1535)$ resonance – see Fig. 1 – with the $N^*(1535)$ coming with narrower momentum distribution compared to nucleons [36, 37].

Earlier bound state searches at COSY, assuming the above mechanism, focused on the reaction $dd \rightarrow {}^3\text{He}N\pi$. The excitation functions determined around the threshold for $dd \rightarrow {}^4\text{He}\eta$ did not reveal a structure that could be interpreted as a narrow mesic nucleus [8, 38–40]. Upper limits for the total cross sections for bound state production and decay in the processes $dd \rightarrow ({}^4\text{He}\text{-}\eta)_{\text{bound}} \rightarrow {}^3\text{He}n\pi^0$ and $dd \rightarrow ({}^4\text{He}\text{-}\eta)_{\text{bound}} \rightarrow {}^3\text{He}p\pi^-$ were deduced to be about 5 nb and 10 nb for the $n\pi^0$ and $p\pi^-$ channels, respectively [38]. The bound state production cross sections for $pd \rightarrow ({}^3\text{He}\text{-}\eta)_{\text{bound}}$ [41] are expected to be more than 20 times larger than for $dd \rightarrow ({}^4\text{He}\text{-}\eta)_{\text{bound}}$ [42].

II. EXPERIMENT

A. Measurement conditions

The high statistics experiment devoted to the search for ${}^3\text{He}\text{-}\eta$ mesic nuclei in the $pd \rightarrow dp\pi^0$ reaction was carried out with the WASA (Wide Angle Shower Apparatus) [16, 30–33] detection setup installed at the COSY accelerator [28, 29]. The WASA detector consisted of two main parts: the Forward Detector (FD) and Central Detector (CD) optimized for tagging the recoil particles and registering the meson decay products, respectively.

The measurement was performed changing the proton beam momentum very slowly and continuously around the η production threshold in each acceleration cycle from 1.426 to 1.635 GeV/c, corresponding to the ${}^3\text{He}\eta$ excess energy range $Q \in (-70, 30)$ MeV ($Q = \sqrt{s_{pd}} - m_\eta - m_{{}^3\text{He}}$, where $\sqrt{s_{pd}}$ is invariant mass of colliding proton and deuteron). The application of this so-called ramped beam technique allowed us to reduce the systematic uncertainties with respect to separate runs at fixed beam energies [8, 43].

Possible resonance-like structure below the η production threshold associated with the ${}^3\text{He}\text{-}\eta$ bound state was searched for via measurement of the excitation function for the $pd \rightarrow dp\pi^0$ reaction.

B. $pd \rightarrow ({}^3\text{He}\text{-}\eta)_{\text{bound}} \rightarrow dp\pi^0$ events selection

The events corresponding to formation of ${}^3\text{He}\text{-}\eta$ bound states were selected with appropriate conditions based on the Monte Carlo simulation of the $pd \rightarrow ({}^3\text{He}\text{-}\eta)_{\text{bound}} \rightarrow dp\pi^0$ reaction. The considered kinematic mechanism of the process is presented schematically in Fig. 1. According to the scheme, the proton deuteron collision leads to

the formation of a ${}^3\text{He}$ nucleus bound with the η meson via strong interactions. Then, the η meson can be absorbed by one of the nucleons inside the helium exciting it to the $N^*(1535)$ nucleon resonance until the resonance decays into a proton π^0 pair, with the pion subsequently decaying into two photons. This mechanism, with formation of an intermediate N^* , was also assumed in the previous analyses [8, 38–40].

The simulation was performed using the N^* resonance momentum distribution in the N^* -deuteron system determined recently by Kelkar et al. [36, 37]. The distribution calculated for two different values of binding energy $E_{N^*-d} = -0.33$ MeV and -0.53 MeV is shown in Fig. 2 (red solid and green dashed lines). It is much narrower compared to the Fermi momentum distribution of protons inside ${}^3\text{He}$ [44] (blue dotted line) which results from the fact that the N^* binding energy is smaller than the energy separation of proton in ${}^3\text{He}$.

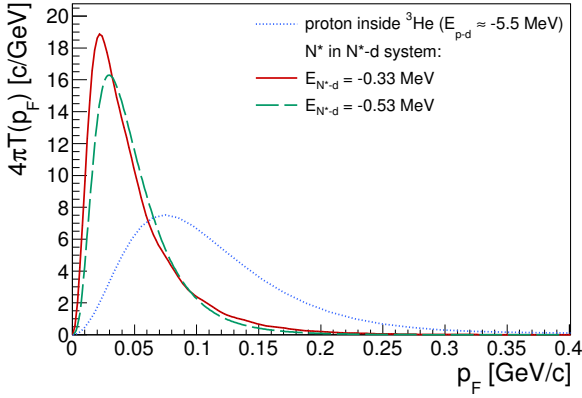


FIG. 2: (Color online) Fermi momentum distribution of the N^* resonance in the N^* -deuteron bound state for two different values of binding energy $E_{N^*-d} = -0.33$ MeV and -0.53 MeV (red solid and green dashed lines, respectively) [36, 37] and of protons inside ${}^3\text{He}$ nucleus for the separation energy ≈ 5.5 MeV (blue dotted line) [44].

The deuteron in this process plays the role of a spectator. In the simulations it was assumed that the bound state has a resonance structure given by the Breit-Wigner distribution with fixed binding energy B_s and width Γ :

$$N(\sqrt{s_{pd}}) = \frac{\Gamma^2/4}{(\sqrt{s_{pd}} - (m_\eta + m_{{}^3\text{He}} - B_s))^2 + \Gamma^2/4}, \quad (1)$$

where $\sqrt{s_{pd}}$ is the invariant mass of the colliding proton and deuteron and $m_\eta + m_{{}^3\text{He}} - B_s$ is the bound state mass. The total invariant mass $\sqrt{s_{pd}}$ was calculated based on the proton beam momentum p_{beam} , which was generated with uniform probability density distribution in the range of $p_{beam} \in (1.426, 1.635)$ GeV/c corresponding to the experimental beam ramping.

Events selection for the $pd \rightarrow ({}^3\text{He}-\eta)_{bound} \rightarrow dp\pi^0$ process started with particles identification in the Central

Detector. Protons were identified based on the energy deposited in the Scintillator Electromagnetic Calorimeter (SEC) combined with the energy loss in the Plastic Scintillator Barrel (PSB), see Fig. 3.

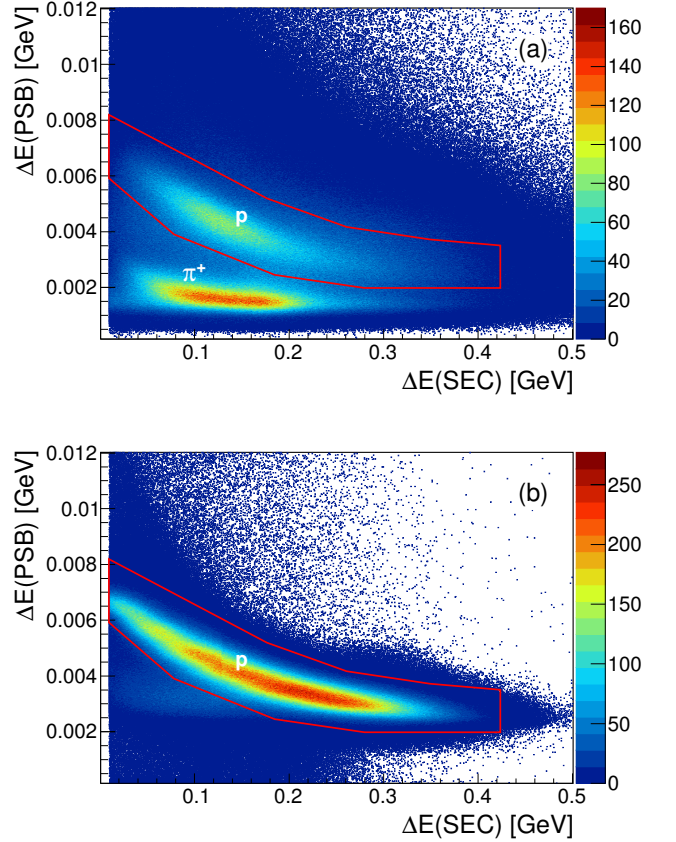


FIG. 3: (Color online) Energy deposited in the Scintillator Electromagnetic Calorimeter (SEC) as a function of the energy loss in the Plastic Scintillator Barrel (PSB) for experimental data (a) and simulations (b). The area corresponding to selected protons is marked with a red solid line.

The neutral pions π^0 were identified on the basis of the invariant mass of two photons originating from their decays and measured in the SEC (Fig. 4(a)).

Deuterons which were not directly registered in the experiment were identified via the missing mass technique. The events corresponding to η -mesic bound states were selected by applying cuts in the π^0 -proton opening angle in the c.m. frame $\vartheta_{\pi^0,p}^{c.m.}$, in the missing mass as well as in the deuteron momentum p_d distributions. The spectra including experimental data and Monte-Carlo simulation for the signal and the dominant background $pd \rightarrow dp\pi^0$ process are presented in Fig. 4 with marked selection cuts.

The final number of selected events as a function of the excess energy Q for the $pd \rightarrow dp\pi^0$ reaction is shown in Fig. 5. The excess energy range $Q \in (-70, 30)$ MeV was divided into 40 intervals, each of width 2.5 MeV.

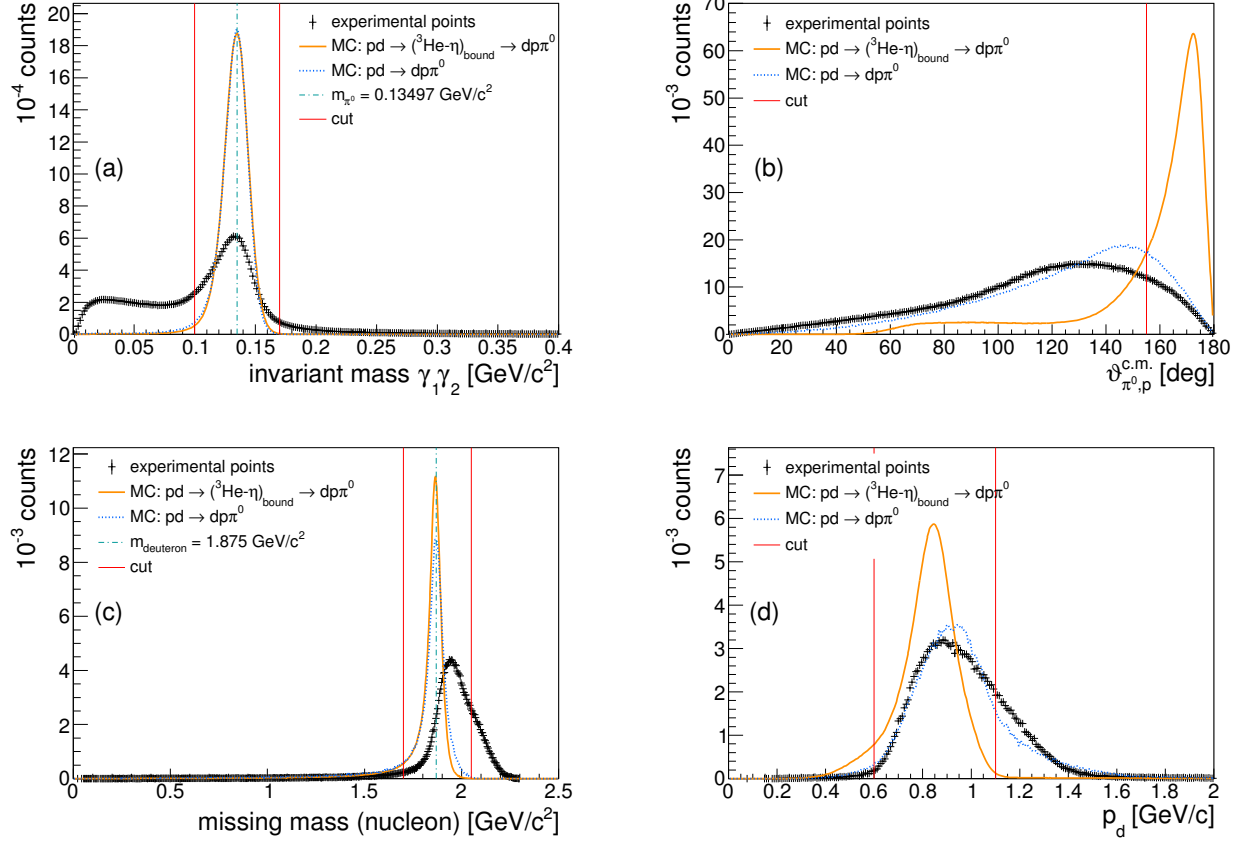


FIG. 4: (Color online) (a) π^0 identification based on the two photon invariant mass spectrum, (b) π^0 -proton opening angle in the c.m. frame $\vartheta_{\pi^0,p}^{\text{c.m.}}$, (c) deuteron identification based on the missing mass technique, (d) the deuteron momentum distribution in the laboratory frame p_d . Data are shown as black crosses. Orange solid and blue dotted curves show the simulation of signal and background from $pd \rightarrow dp\pi^0$ reaction respectively, while the red vertical lines indicate the boundary of the applied selection cuts.

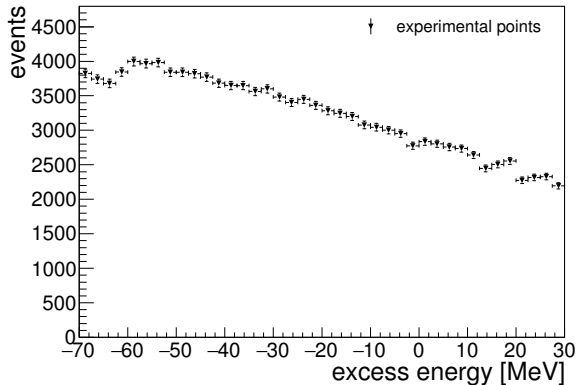


FIG. 5: The number of selected events for the $pd \rightarrow dp\pi^0$ reaction after application of all selection criteria.

C. Luminosity and efficiency

In order to determine the excitation function for the studied reaction the number of events in each excess energy interval has to be normalized by the integrated luminosity and corrected for the total efficiency. Since, during the beam ramping process the luminosity has varied due to the change of the beam-target overlap, the luminosity dependence on the excess energy $L(Q)$ has been determined analysing the quasi-elastic proton-proton scattering process based on the method described in [45, 46]. For this purpose dedicated Monte Carlo simulation for $pd \rightarrow ppn_{spectator}$ reaction has been performed assuming that the beam protons scatter on the protons in the deuteron target and the neutrons from the deuteron play a role of spectators. The target nucleons momenta were generated isotropically with Fermi momentum distribution derived from the Paris [47] and the CDBonn potential models [48], see Fig. 6.

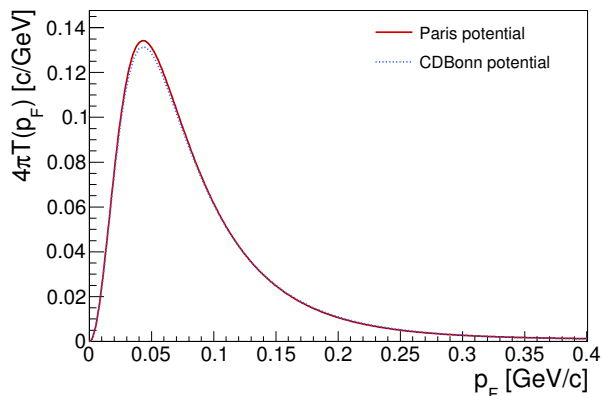


FIG. 6: (Color online) Fermi momentum distribution of nucleons inside the deuteron for Paris (red solid line) [47] and CDBonn (blue dotted line) [48] potential models.

In the analysis quasi-elastically scattered protons were searched for with the primary events selection condition of exactly one charged particle in the Forward Detector and one charged particle in the Central Detector. Proton identification in the Central Detector was based on the selection criterium shown in Fig. 3.

A part of the background from elastic $pd \rightarrow pd$ scattering corresponding to deuterons was subtracted applying the criterium for polar angle $\theta_{CD} \in (40, 100)$ deg, while part corresponding to protons was eliminated by fitting the θ_{CD} distribution for each interval of excess energy Q and polar angle θ_{FD} with the sum of two Gaussian functions (see Fig. 7(d)).

In order to determine the integrated luminosity the number of reconstructed events obtained from Monte Carlo simulation was weighted with the values of the differential cross section for the quasi-free proton-proton scattering, which is uniquely determined by the scattering angle and the total proton-proton collision energy. For the estimation of the differential cross-sections the data for elastic proton-proton scattering [49–51] has been used (see Fig. 8(a)). The integrated luminosity dependence on the excess energy is presented in Fig. 8(b) and its total value is equal to $2511 \pm 2(stat.) \pm 120(syst.) \pm 100(norm.) \text{ nb}^{-1}$, where the statistical, systematic and normalization errors are indicated, respectively. In the calculations the shadowing effect equals 4.5% [52] caused by the neutron shading the scattered protons. The total integrated luminosity is consistent within systematic and normalization errors with the luminosity determined for the current experiment based on two alternative methods presented in Refs. [35, 53].

The Monte Carlo simulations for the $pd \rightarrow (^3\text{He}-\eta)_{bound} \rightarrow dp\pi^0$ process allowed one to determine detection and reconstruction efficiency as a function of the excess energy Q . The obtained geometrical acceptance is equal to about 30% while the full efficiency including all applied selection criteria is about 9% (see Fig. 9).

D. Upper limit of the total cross section

The final excitation function (Fig. 10) was obtained by correcting the number of events identified as $pd \rightarrow (^3\text{He}-\eta)_{bound} \rightarrow dp\pi^0$ for the efficiency (Fig. 9) and normalizing by the luminosity (Fig. 8(b)). The excitation curve does not show any structure that could be interpreted as an indication for the η -mesic ^3He .

Hence, the upper limit of the total cross-section for the $^3\text{He}-\eta$ bound state production and its decay to $dp\pi^0$ channel was evaluated. In order to quantitatively estimate the upper limit, a fit to the excitation function with a polynomial describing the background (first and second order) combined with a Breit-Wigner function (for the signal) was performed. In the fit the polynomial coefficients and the normalization of the Breit-Wigner amplitude were treated as free parameters, while the binding energy B_s

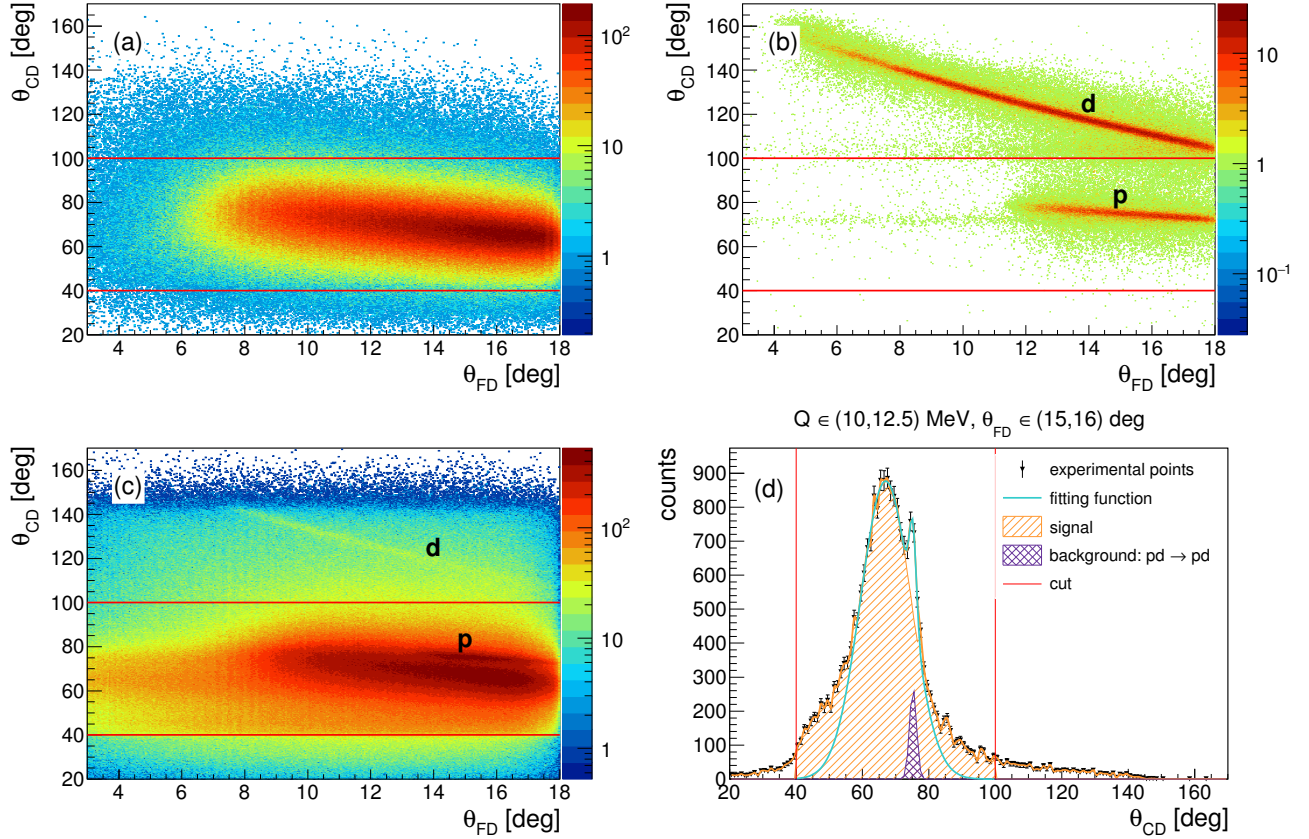


FIG. 7: (Color online) Correlations between the polar angles of charged particles registered in the FD θ_{FD} and CD θ_{CD} obtained in the MC simulations for the $pd \rightarrow ppn_{spectator}$ (a) and $pd \rightarrow pd$ (b) reactions, experimental data (c). Note that the 2D spectra are in logarithmic scale. The applied cut is marked with red horizontal line. The (d) panel shows an example of experimental distribution of θ_{CD} (black points), fitting function (cyan solid curve), signal from $pd \rightarrow ppn_{spectator}$ reaction (orange (light gray) area) and peak from background reaction $pd \rightarrow pd$ (purple checkered area) for $Q \in (10, 12.5)$ MeV and $\theta_{FD} \in (15, 16)$ deg. The applied cut ($\theta_{CD} \in (40, 100)$ deg) is marked with red vertical lines.

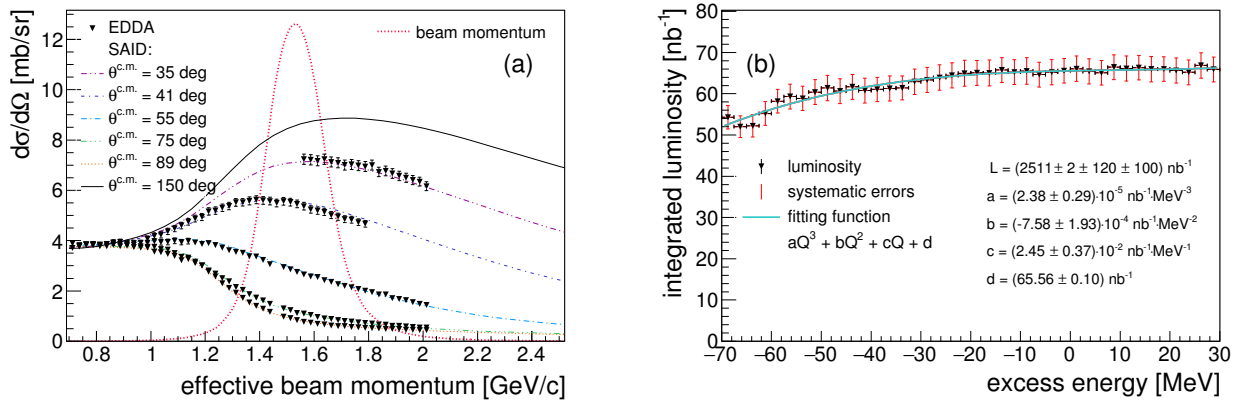


FIG. 8: (Color online) (a) Differential cross sections for proton-proton elastic scattering as a function of the effective beam momentum for different values of the scattering angle $\theta^{c.m.}$ in the c.m. frame. Triangles show EDDA collaboration data [51]. Curves denote SAID calculations [49, 50]. The pink dotted line presents the distribution of the effective beam momentum obtained from simulations. (b) Integrated luminosity calculated based on experimental data for quasifree $pd \rightarrow ppn_{spectator}$ reaction with statistical (black points) and systematic (red vertical bars) errors fitted with third degree polynomial function (cyan curve).

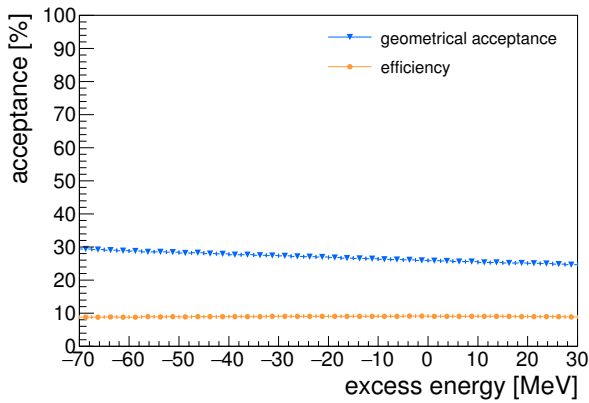


FIG. 9: (Color online) Geometrical acceptance (blue triangles) and efficiency (orange circles) for the $pd \rightarrow (^3\text{He}-\eta)_{\text{bound}} \rightarrow dp\pi^0$ reaction as a function of excess energy.

and the width Γ were fixed in the range from -40 MeV to 0 MeV and from 5 MeV to 50 MeV, respectively. An example excitation function with the fit result for binding energy -30 MeV and width 15 MeV is presented in Fig. 10.

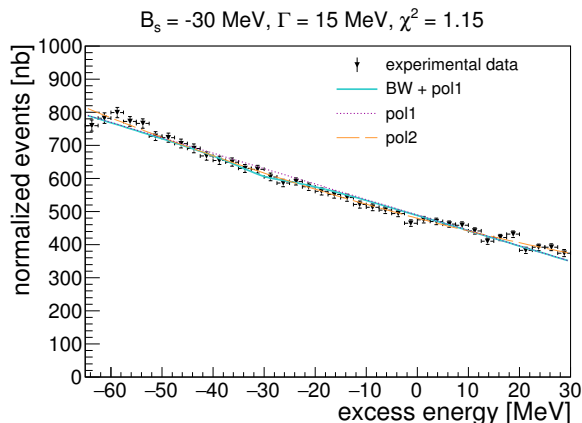


FIG. 10: (Color online) Experimental excitation function for the $pd \rightarrow dp\pi^0$ process obtained after applying the selection criteria described in the text, correction by the efficiency, and normalization by the corresponding integrated luminosity. The cyan solid line represents a fit with a first order polynomial combined with a Breit-Wigner function with fixed binding energy and width equal to -30 MeV and 15 MeV, respectively. The purple dotted and orange dashed lines show the first and second order polynomial (describing the background), respectively.

The upper limit of the total cross section was determined based on the uncertainty of the amplitude obtained from the fit $\Delta\sigma_A$:

$$\sigma_{\text{upper}}^{CL=90\%}(B_s, \Gamma) = k \cdot \Delta\sigma_A, \quad (2)$$

where k is the statistical factor equal to 1.64 corresponding to 90% confidence level (CL) as given by the Particle

Data Group, PDG [54].

The upper limit obtained by averaging the results derived from fits with a background described by the linear and quadratic functions for different values of B_s and Γ is presented in Table I. It varies between 13 to 24 nb and depends mainly on the width of the bound state while is not sensitive to the binding energy. The result for $B_s = -30$ MeV is shown in Fig. 11. The blue checkered area denotes the systematic errors described in the next section. The obtained upper limit as a function of B_s and Γ is presented in Fig. 12.

TABLE I: The upper limit for the cross section for the bound state formation and decay in the $pd \rightarrow (^3\text{He}-\eta)_{\text{bound}} \rightarrow dp\pi^0$ process, determined at the 90% confidence level. The values were obtained by fitting excitation curve with a Breit-Wigner function combined with the first and second order polynomial with different fixed bound state parameters, B_s and Γ .

B_s [MeV]	Γ [MeV]	$\sigma_{\text{upper}}^{CL=90\%}$ [nb]	B_s [MeV]	Γ [MeV]	$\sigma_{\text{upper}}^{CL=90\%}$ [nb]
-40	5	19.74	-20	5	16.85
-40	10	16.08	-20	10	13.64
-40	20	15.61	-20	20	13.19
-40	30	17.35	-20	30	14.86
-40	40	20.14	-20	40	17.86
-40	50	23.67	-20	50	22.21
-30	5	17.91	-10	5	16.11
-30	10	14.34	-10	10	13.07
-30	20	13.49	-10	20	12.67
-30	30	14.66	-10	30	14.23
-30	40	16.85	-10	40	16.96
-30	50	19.92	-10	50	20.79

E. Systematics

Systematic checks were performed just as in the previous analyses presented in Refs. [8, 38]. The upper limit of the total cross section obtained in the $pd \rightarrow (^3\text{He}-\eta)_{\text{bound}} \rightarrow dp\pi^0$ reaction analysis is sensitive to the variation of the selection criteria, systematic error of the luminosity determination, and application of different theoretical models.

Changing the selection criteria applied in analysis within $\pm 10\%$ results in the systematic error of about 8.5% .

Overall systematic and normalization errors of the luminosity determined based on the quasi-free pp reaction are equal to 4.8% and 4% , respectively, and are another contribution to the systematic uncertainty of the upper limit.

The description of the background with quadratic and linear functions introduces additional systematic uncer-

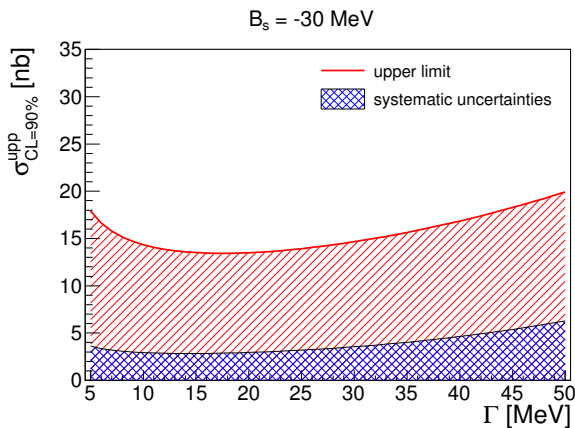


FIG. 11: (Color online) The upper limit at the 90% confidence level of the total cross section for formation of the ${}^3\text{He}\text{-}\eta$ bound state and its decay via the $pd \rightarrow ({}^3\text{He}\text{-}\eta)_{\text{bound}} \rightarrow dp\pi^0$ reaction as a function of the width of the bound state. The binding energy was fixed to $B_s = -30$ MeV. The blue checkered area at the bottom represents the systematic uncertainties.

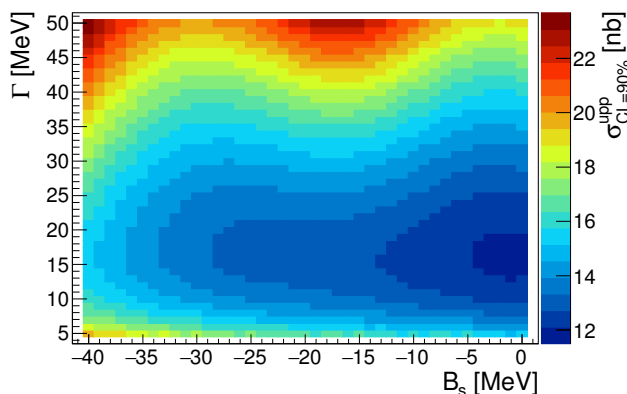


FIG. 12: (Color online) The upper limit of the total cross section at the 90% confidence level obtained based on excitation curves fit assuming different bound state parameters, B_s and Γ .

tainty, which is estimated as

$$\delta = \frac{\sigma_{quad} - \sigma_{lin}}{2}. \quad (3)$$

This systematic error changes from about 2% (for $\Gamma = 5$ MeV) to 24% ($\Gamma = 50$ MeV).

An important source of systematic errors comes from the assumption of the N^* momentum distribution inside the ${}^3\text{He}$ nucleus applied in the simulations. The current analysis was performed with the Fermi momentum distribution for N^* determined for binding energy -0.53 MeV by Kelkar et al. [36, 37]. In addition, in this analysis the simulations were also performed assuming that the N^* resonance in the c.m. frame moves with a momentum distribution similar to that of protons inside ${}^3\text{He}$ [44] (see

the blue dotted line in Fig. 2). The choice of the alternative model does not influence the experimental method but it affects the acceptance of the deuterons in the FD, which is connected with the fact that the momentum distribution of protons inside ${}^3\text{He}$ is peaked at higher value with respect to the N^* distribution in the $N^*\text{-}d$ system. It provides a systematic error of about 17%.

Adding the above-estimated contributions in quadrature we obtain systematic uncertainty of the upper limit that varies from 20% to 31%. The systematic uncertainties are presented by the blue checkered area in Fig. 11.

III. CONCLUSION

In order to search for evidence of a possible ${}^3\text{He}\eta$ bound state we performed measurements of the proton beam scattering on a deuteron target with the WASA-at-COSY detector. The analysis was based on the determination of the excitation function for the $pd \rightarrow dp\pi^0$ process. The applied selection criteria were inferred from Monte-Carlo simulations based on the assumption that the N^* resonance momentum in the $N^*\text{-deuteron}$ bound state is distributed according to the recent theoretical modelling in [36, 37].

Narrow resonance-like structure associated with an η -mesic ${}^3\text{He}$ bound state was not observed. Therefore, the upper limit for the total cross sections for the $pd \rightarrow ({}^3\text{He}\text{-}\eta)_{\text{bound}} \rightarrow dp\pi^0$ process was estimated and varies from 13 to 24 nb depending on the bound state parameters $B_s \in (0, 40)$ MeV and $\Gamma \in (0, 50)$ MeV.

The upper limit obtained in this analysis for the $pd \rightarrow ({}^3\text{He}\text{-}\eta)_{\text{bound}} \rightarrow dp\pi^0$ reaction is about 3 times lower than the limit of 70 nb [7, 55] determined by the COSY-11 collaboration for the $pd \rightarrow ({}^3\text{He}\text{-}\eta)_{\text{bound}} \rightarrow {}^3\text{He}\pi^0$ process. The limit about 24 nb found here compares with the total cross section for η meson production above threshold in dp collisions which is about 400 nb [43]. In dd collisions the limits obtained by the WASA-at-COSY Collaboration for the $dd \rightarrow {}^3\text{He}n\pi^0$, $dd \rightarrow {}^3\text{He}p\pi^-$ processes (2.5 – 7 nb) [8, 38] compare with the total cross section 15 nb [56] for η production above threshold. These measurements provide an important constraint for models of $\text{He}\text{-}\eta$ bound state production. Within the limits determined here, bound states predicted with η -nucleon scattering lengths about 1 fm remain a possibility.

Acknowledgments

We acknowledge the support from the Polish National Science Center through grant No. 2016/23/B/ST2/00784. Theoretical parts of this work was partly supported by the Faculty of Science, Universidad de los Andes, Colombia, through project number P18.160322.001-17, and by JSPS KAKENHI Grant Numbers JP16K05355 (S.H.) in Japan.

-
- [1] Q. Haider and L. C. Liu. *Phys. Lett. B*, 172(2):257, 1986.
 - [2] N. G. Kelkar. *Phys. Lett. B*, 709(1-2):21, 2012.
 - [3] V. A. Baskov, A. V. Koltsov, A. I. L'vov, A. I. Lebedev, L. N. Pavlyuchenko, V. V. Polyanskiy, E. V. Rzhano, S. S. Sidorin, G. A. Sokol, S. V. Afanasiev, A. I. Malakhov, A. S. Ignatov, and V. G. Nedorezov. *PoS Baldin-ISHEPP-XXI*, page 102, 2012.
 - [4] R. E. Chrien et al. *Phys. Rev. Lett.*, 60(25):2595, 1988.
 - [5] A. Budzanowski et al. *Phys. Rev. C*, 79(1):012201, 2009.
 - [6] S. V. Afanasiev et al. *Phys. Part. Nucl. Lett.*, 8:1073, 2011.
 - [7] P. Moskal and J. Smyrski. *Acta Phys. Pol. B*, 41(10):2281, 2010.
 - [8] P. Adlarson et al. *Phys. Rev. C*, 87(3):035204, 2013.
 - [9] N. G. Kelkar, K. P. Khemchandani, N. J. Upadhyay, and B. K. Jain. *Rept. Prog. Phys.*, 76:066301, 2013.
 - [10] V. Metag, M. Nanova, and E. Ya. Paryev. *Prog. Part. Nucl. Phys.*, 97:199, 2017.
 - [11] S. Bass and P. Moskal. *Rev. Mod. Phys.*, 91:015003, 2019.
 - [12] B. Krusche and C. Wilkin. *Prog. Part. Nucl. Phys.*, 80:43, 2015.
 - [13] C. Wilkin. *Eur. Phys. J. A*, 53:114, 2017.
 - [14] M. Skurzok. *arXiv:2004.13467*, 2020.
 - [15] M. Pfeiffer et al. *Phys. Rev. Lett.*, 92(25):252001, 2004.
 - [16] P. Adlarson et al. *Phys. Lett. B*, 782:297, 2018.
 - [17] T. E. O. Ericson and W. Weise. *Int. Ser. Monogr. Phys., Oxford UP*, 74, 1988.
 - [18] N. Barnea, B. Bazak, E. Friedman, and A. Gal. *Phys. Lett. B*, 771:297, 2017.
 - [19] N. Barnea, E. Friedman, and A. Gal. *Nucl. Phys. A*, 968:35, 2017.
 - [20] A. Fix and O. Kolesnikov. *Phys. Lett. B*, 772:663, 2017.
 - [21] J.-J. Xie, W.-H. Liang, E. Oset, P. Moskal, M. Skurzok, and C. Wilkin. *Phys. Rev. C*, 95(1):015202, 2017.
 - [22] M. Nanova et al. *Phys. Lett. B*, 727(4-5):417, 2013.
 - [23] Y. K. Tanaka et al. *Phys. Rev. Lett.*, 117(20):202501, 2016.
 - [24] S. D. Bass and A. W. Thomas. *Phys. Lett. B*, 634(4):368, 2006.
 - [25] S. D. Bass and A. W. Thomas. *Acta Phys. Polon. B*, 45(3):627, 2014.
 - [26] A. V. Anisovich, V. Burkert, M. Dugger, E. Klempt, V. A. Nikonov, B. Ritchie, A. V. Sarantsev, and U. Thoma. *Phys. Lett. B*, 785:626, 2018.
 - [27] E. Czerwinski et al. *Phys. Rev. Lett.*, 113(6):062004, 2014.
 - [28] R. Maier. *Nucl. Instrum. Meth. A*, 390(1-2):1, 1997.
 - [29] D. Prasuhn. *IKP Annual Report*, 2006.
 - [30] H.-H. Adam et al. *arXiv:nucl-ex/0411038*, 2004.
 - [31] Chr. Bargholtz et al. *Nucl. Instrum. Meth. A*, 594(3):339, 2008.
 - [32] P. Adlarson et al. *Phys. Rev. C*, 90(4):045207, 2014.
 - [33] Chr. Bargholtz et al. *Nucl. Instrum. Meth. A*, 587(2-3):178, 2008.
 - [34] M. Skurzok, S. Hirenzaki, S. Kinutani, H. Konishi, P. Moskal, H. Nagahiro, and O. Rundel. *Nucl. Phys. A*, 993:121647, 2020.
 - [35] P. Adlarson et al. *Phys. Lett. B*, 802:135205, 2020.
 - [36] N. Kelkar, H. Kamada, and M. Skurzok. *Int. J. Mod. Phys. E*, 28(8):1950066, 2019.
 - [37] N. Kelkar, D. Bedoya Fierro, H. Kamada, and M. Skurzok. *Nucl. Phys. A*, 996:121698, 2020.
 - [38] P. Adlarson et al. *Nucl. Phys. A*, 959:102, 2017.
 - [39] M. Skurzok, P. Moskal, N. G. Kelkar, S. Hirenzaki, H. Nagahiro, and N. Ikeno. *Phys. Lett. B*, 782:6, 2018.
 - [40] M. Skurzok. *Acta Phys. Polon. B*, 51(1):33, 2020.
 - [41] C. Wilkin. *Acta Phys. Polon. B*, 45(3):603, 2014.
 - [42] S. Wycech and W. Krzemien. *Acta Phys. Polon. B*, 45(3):745, 2014.
 - [43] J. Smyrski et al. *Phys. Lett. B*, 649(4):258, 2007.
 - [44] A. Nogga, A. Kievsky, H. Kamada, and W. Gl'Phys. Rev. C, 67(3):034004, 2003.
 - [45] P. Moskal and R. Czyżykiewicz. *AIP Conf. Proc.*, 950(1):118, 2007.
 - [46] A. Khreptak, O. Rundel, and M. Skurzok. *EPJ Web of Conferences*, 199:05026, 2019.
 - [47] M. Lacombe, B. Loiseau, R. Vinh Mau, J. Coté, P. Pirés, and R. de Tourreil. *Phys. Lett. B*, 101(3):139, 1981.
 - [48] R. Machleidt. *Phys. Rev. C*, 63(2):024001, 2001.
 - [49] R. A. Arndt, W. J. Briscoe, I. I. Strakovsky, and R. L. Workman. *Phys. Rev. C*, 76(2):025209, 2007.
 - [50] SAID database: <http://gwdac.phys.gwu.edu/>. The CNS Data Analysis Center.
 - [51] D. Albers, J. Bisplinghoff, R. Bollmann, K. Busser, P. Cloth, R. Daniel, O. Diehl, F. Dohrmann, H. P. Engelhardt, and J. Ernst. *Phys. Rev. Lett.*, 78(9):1652, 1997.
 - [52] E. Chiavassa et al. *Phys. Lett. B*, 337(1-2):192, 1994.
 - [53] O. Rundel. *arXiv:1905.04544*, 2019.
 - [54] M. Tanabashi et al. *Phys. Rev. D*, 98(3):030001, 2018.
 - [55] J. Smyrski et al. *Nucl. Phys. A*, 790(1-4):438c, 2007.
 - [56] N. Willis et al. *Phys. Lett. B*, 406(1-2):14, 1997.